Thin Solid Films, 396 (2001) 1-2, 78-83

Transmission electron microscopy investigation of Fe_3O_4 films grown on (111) Pt substrates.

V.V. Roddatis[1], D.S. Su[*], C. Kuhrs, W. Ranke and R. Schlögl

On leave from Institute of Crystallography, Russian Academy of Sciences, Leninskii pr.59, 117333, Moscow, Russia

Department of Inorganic Chemistry, Fritz-Haber-Institute of the MPG, Faradayweg 4-6, 14195 Berlin, Germany

[*] Corresponding author: e-mail dangsheng@fhi-berlin.mpg.de, phone +49 30 8413 5406

Received 12 October 2000; accepted 22 June 2001

Abstract

Thin Fe_3O_4 films prepared by iron deposition and subsequent oxidation on Pt(111) single crystal substrates were studied by selected area electron diffraction and high-resolution transmission electron microscopy (HRTEM). No other iron oxide phases were detected. The formation of Fe_3O_4 films takes place epitaxially on Pt(111) substrates with the relationships: $[111]_{Pt}$ // $[111]_{Fe3O4}$, $[1\bar{1}0]_{Pt}$ // $[1\bar{1}0]_{Fe3O4}$. The films were free of dislocations but contained antiphase boundaries (APB) between domains shifted by 1.86Å or 2.35Å relative to each other along the [111] direction. The lattice mismatch between Fe_3O_4 and Pt causes periodic arrays of strained regions in the oxide along the interface. The iron oxide lattice parameters near the interface are compressed by approximately 2%. Detailed analysis of the Pt-Fe_3O_4 interface based on HRTEM images and image simulations show that the first layer of the oxide on the Pt substrate consists of iron atoms.

Keywords: Iron oxide, Platinum, Structural properties, TEM

Introduction

Iron oxides are widely used as catalytic materials for a number of important chemical processes [1], for instance potassium promoted Fe_2O_3 is used as a catalyst for the dehydrogenation of ethylbenzene to styrene [2,3]. Magnetic oxide multilayers of Fe_3O_4 combined with other oxides are used to study magnetic coupling across nonmagnetic barriers and between antiferromagnetic layers [4]. These properties are also important for the development of magnetic-field sensors and high-density magnetic recording media [5].

Highly ordered metal oxide films can be prepared, for example, by oxidizing the surface region of corresponding metal crystals [6], by repeated deposition of the metal and subsequent oxidation [7-10], by molecular-beam epitaxy [11] or by reactive vapor deposition [12]. The selective growth of α-Fe_2O_3 and Fe_3O_4 is determined by the growth rate and the oxygen partial pressure. Moreover, during the growth these phases can transform into each other depending on the ambient conditions.

The growth of iron-oxide films on different substrates has been studied in a number of works. However, up to now mainly scanning tunneling microscopy (STM) and low energy electron diffraction (LEED) has been employed to study the initial growth stages and surface structure [7,10,11,13-15]. Information about the bulk including structure, density and nature of defects (with the exception of point defects), can be obtained from transmission electron microscopy (TEM). So far, such investigations have only been carried out to study the influence of the structure of Fe_3O_4 films grown on MgO on their magnetic properties [16]. It has been found that the presence of APBs causes an anomalous high field behavior. But the structure of these defects was not investigated in detail.

The preparation of iron oxide films on Pt substrates starts always with the formation of a thin FeO-like

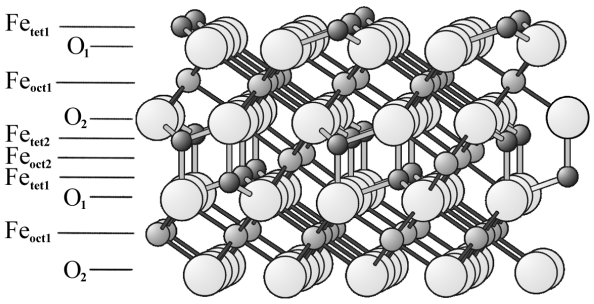

Fig. 1. Perspective view of the Fe_3O_4 structure exposing a (111) surface plane without relaxation. The lattice consists of the close-packed oxygen layers O_1 and O_2, separated by different iron layers, the "Kagome-layer", Fe_{oct1}, and the "mixed trigonal layer " consisting of Fe_{tet1}, Fe_{oct2} and Fe_{tet2}.

layer [10]. These films are prepared under conditions near the thermodynamic phase boundary separating the stable regions of α-Fe_2O_3 and Fe_3O_4 [17]. Therefore, it remains to be seen whether an FeO phase still exists at the interface between the thick Fe_3O_4 film and the Pt substrate and whether the thick film contains Fe_2O_3-domains. The lattice mismatch between Pt(111) and Fe_3O_4(111) is about 7% and surface structure studies suggest that the oxide layer grows aligned but not in registry with the atomic rows of the substrate. It is unknown, if this growth mode also applies to the region near the interface or if the oxide grows epitaxially first and then releases the strain in a dislocation network not visible at the surface. These questions are tackled by the detailed structural investigation presented here using electron diffraction and HRTEM.

Platinum exhibits a cubic fcc structure with the space group Fm3m, the lattice parameter a = 0.39nm. Fe_3O_4 crystallizes in a cubic inverse spinel structure (space group Fd3m, a=0.84nm) [18]. As shown in Fig. 1, the iron atoms occupy interstitial sites of the close-packed fcc sublattice of oxygen anions. The layer Fe_{oct1} ("Kagome-layer") contains divalent ions in octahedral sites. The "mixed trigonal layer" consists of the three sublayers Fe_{tet1}, Fe_{oct2} and Fe_{tet2} and contains divalent and trivalent ions.

Experimental

The experiments were performed in an ultra-high-vacuum chamber with a base pressure of 10^{-10}mbar. As described in detail in [19] this chamber is equipped with a commercial STM head (Burleigh Instruments), backview LEED optics (Omicron) and a cylindrical mirror analyzer for Auger electron spectroscopy (Omicron). The Pt(111) surface was prepared by repeated cycles of argon ion bombardment and subsequent annealing at 1300K until it exhibited a sharp LEED pattern and no contamination signals can be detected in the Auger electron spectrum. About one monolayer (ML) of iron was then deposited by resistively heating a tungsten wire with an iron wire wrapped around it, followed by oxidation in 10^{-6} mbar oxygen at 1020K. This creates a well ordered film consisting of one full Fe layer on the Pt substrate terminated towards the vacuum by one full O layer [20]. The iron ions have the valency +2 [21]. Therefore, this film is termed FeO(111). Additionally, the unit cell dimensions are near to those of bulk FeO(111), although slightly expanded [22]. Onto this film, a thick iron film was deposited corresponding to about 20 times the amount necessary for an FeO monolayer. It was oxidized in 10^{-6} mbar oxygen at temperatures increasing slowly from 770K to 1000K. The surface structure of such films was studied in detail in [20].

Plan view specimens for TEM investigations were prepared by mechanical dimpling the Pt substrate down to 20μm followed by ion thinning in a Gatan PIPS system. In order to prepare cross section samples, a piece of glass was glued on the film, to protect it against of damage. The samples were then cut, polished and ion milled until perforation at the Pt-oxide interface. The specimens were examined in a Philips CM200 FEG transmission electron microscope operated at 200kV and in a JEOL 4000EX electron microscope operated at 400kV. All high-resolution image simulations of focus–thickness series were performed using an original program package based on multislice calculations.

Results and discussion

Fig. 2 shows a series of LEED patterns obtained for three stages of preparation of the epitaxial iron oxide film. Complete analysis of such patterns was given in [23].

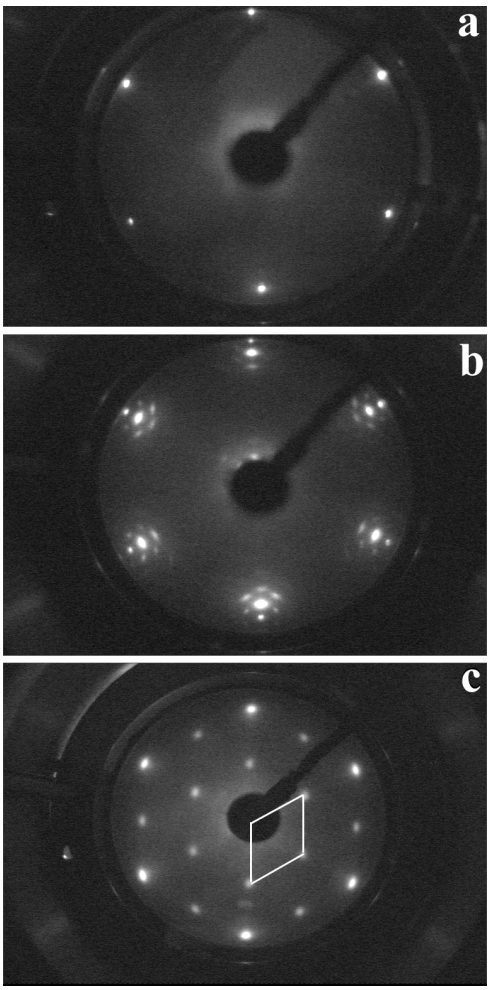

Fig. 2. LEED patterns obtained from (a) a clean Pt(111) surface, (b) an FeO(111) monolayer and (c) an approximately 6 nm thick Fe_3O_4(111) film.

Briefly, Fig. 2a is the pattern of the clean Pt(111) substrate. Upon the deposition of an FeO(111) monolayer (Fig. 2b), additional bright spots from the FeO layer as well as satellites due to multiple diffraction became visible. The LEED pattern of the thick film after the oxidation at high temperature is presented in Fig. 2c. The patterns from the Pt substrate (Fig. 2a) and the oxide film (Fig. 2c) show the same symmetry, while the periodicity in the latter pattern is nearly half of that in Fig. 2a. Detailed analysis confirms that the pattern in Fig. 2c stems from the Fe_3O_4 with a lattice parameter 0.84 nm. Therefore, LEED reveals that the surface of the film was oxidized to form a Fe_3O_4 lattice, with the alignment of the Fe_3O_4 [111] direction parallel to the Pt [111] direction. Since both LEED patterns cannot be seen simultaneously, a slight misorientation of the Fe_3O_4 film with respect to the Pt substrate cannot be ruled out.

In order to elucidate the bulk structure of the film after oxidation, selective area diffraction (SAD) patterns from three mutually perpendicular directions: [111], $[1\bar{1}0]$ and $[11\bar{2}]$ are shown in Fig. 3a, b and c, respectively. Strong bright spots in all diffraction patterns stem from the Pt substrate. They are marked with indices in normal font. Reflexes from the film are rather weak and are indexed in *italic* font. Using the spots of Pt as a reference, the additional weak spots can be identified as reflections of Fe_3O_4. No spots that could be attributed to other iron oxides were found. Therefore, we conclude that the iron film was completely oxidized to Fe_3O_4. Weak spots marked with arrows in Fig. 3a are due to double diffraction. The spots from the Fe_3O_4 film in Figs. 3b and 3c are elongated, revealing a random rotation of the [111] axis (direction normal to the surface) of the oxide film with respect to the substrate within about ±1.5° indicating a mosaic structure of the film. Also, a weak spots occuring from Fe_3O_4 domains rotated by 180º around [111] are marked by arrowheads in Fig. 3b. The presence of such domains was also observed in [20]. Thus, the epitaxial orientational relationships between the Pt substrate and the Fe_3O_4 film determined from SAD patterns are:

$$[111]_{Pt} \,//\, [111]_{Fe3O4}$$

$$[1\bar{1}0]_{Pt} \,//\, [1\bar{1}0]_{Fe3O4}.$$

A cross-sectional HRTEM image along the $[1\bar{1}0]$ direction is shown in Fig. 4a. Over large distances, the Fe_3O_4 film thickness varies from 5 to 7.5nm (see also Fig. 6a). We believe that these variations are mainly due to the nucleation of oxide crystallites during the oxidation process and due to their growth by diffusion of iron atoms across the surface. The thickness variation within the range of several μm is only on the order of a few nm as observed by STM [20]. No voids or cavities were found in the film. Slight changes in contrast of the film are the result of variable thickness and imaging conditions. A simulated through focus series of the Fe_3O_4 structure is shown in Fig. 4b.

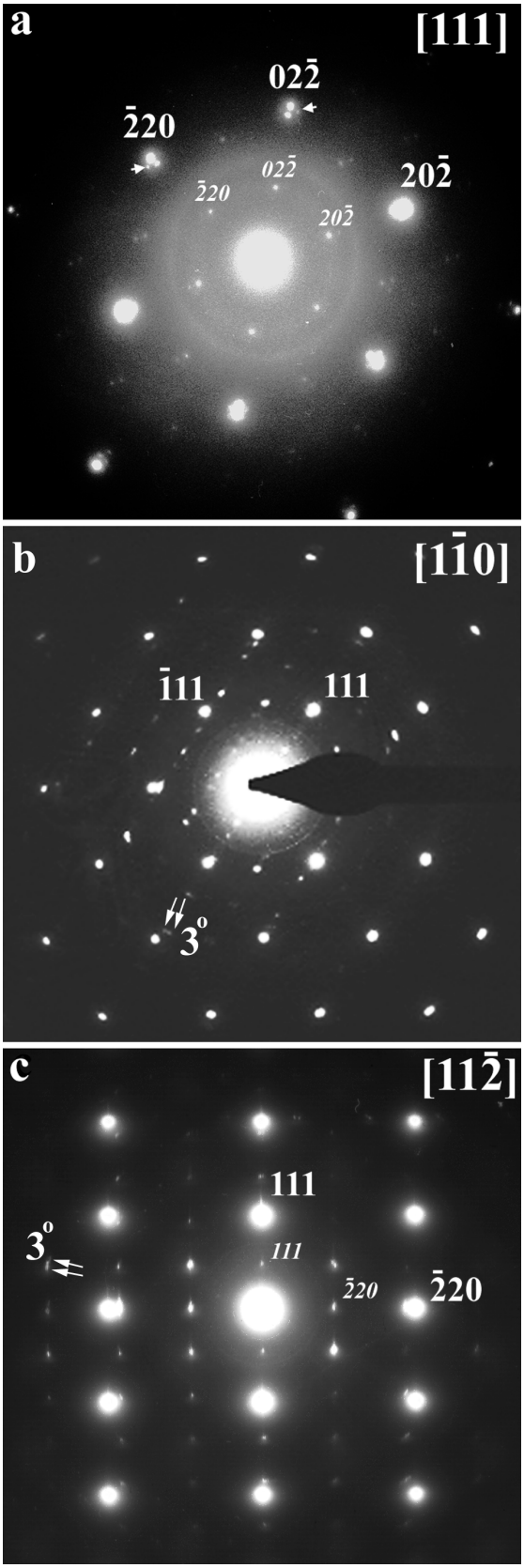

Fig. 3. Selected area diffraction patterns (a) along [111], (b) along $[1\bar{1}0]$ and (c) along $[11\bar{2}]$. Spots corresponding to Pt and Fe_3O_4 are shown with normal and italic font style, respectively. Double diffraction spots are marked with arrows in (a). Reflexes coming from 180º rotated domains are shown by arrowheads in (b).

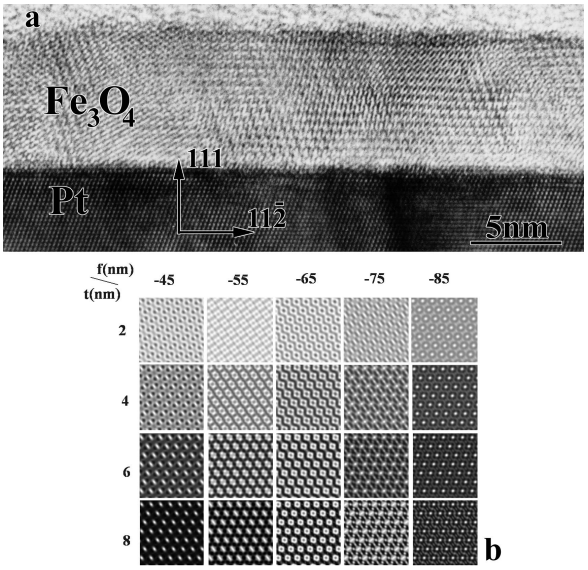

Fig. 4. HRTEM image along $[1\bar{1}0]$; (b) simulated thickness/defocus series for Fe_3O_4 projected along the $[1\bar{1}0]$ direction (U=200kV, C_s=1.15mm, df=5.1nm, sc=0.25mrad).

The obtained knowledge of the epitaxial relationship between the oxide film and the substrate allows elucidation of the interface structure by means of high-resolution imaging and image simulations. An enlarged section of the Fe_3O_4/Pt interface is shown in Fig. 5a. Based on the crystal structure of the oxide shown in Fig. 1 different models of the interface could be constructed and corresponding HRTEM images were simulated for different thickness and defocus values. The best fit between experimental and simulated images was obtained for the unrelaxed model, representing Fe-terminated Fe_3O_4 on Pt (111) (Fig. 5b). In this model iron atoms are in Fe_{oct1} states, octahedrally coordinated to oxygen. The simulated image is shown as an inset in Fig. 5a. This finding is in agreement with the growth procedure of the film described above. It seems that the 6.6% lattice mismatch between Pt and Fe_3O_4 is accommodated in multiple ways. For instance, on flat parts of the interface the lattice of Fe_3O_4 near the interface is compressed over several unit cells: the distance between bright spots marked with black arrowheads (Fig. 5a) at the interface is 2% smaller than that of those marked in the middle of the film. The mismatch accommodation by the formation of misfit dislocations was not observed. Instead, contrast changes with an approximate 2nm periodicity near the interface (Fig. 6a and Fig. 7a) could be attributed to strains and stress variations. In fact, a roughening of the Pt surface by appearence of atomic steps upon formation of the initial FeO monolayer was observed by STM [20]. The frequent observation of steps at the interface in the present work suggests that these steps are conserved during deposition of the thick Fe_3O_4 film and may contribute to its stabilization.

The HRTEM image of the Fe_3O_4 along the [11$\bar{2}$] direction and the corresponding through focus series are shown in Fig. 6a and 6b, respectively. The image simulation shows that

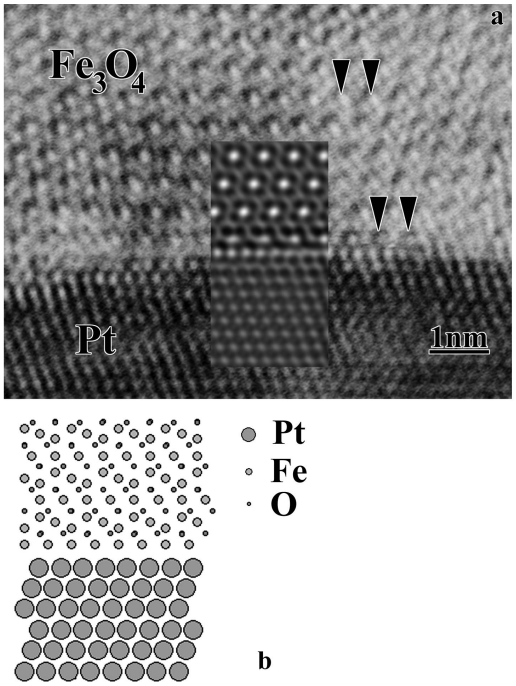

Fig. 5. Enlarged image of the Fe_3O_4/Pt interface with a simulated image shown in the inset. The bright spots marked by arrows near the interface are contracted by 2% compared to corresponding spots marked in the bulk. (b) Atomic model corresponding to the simulated image of the Fe_3O_4/Pt interface.

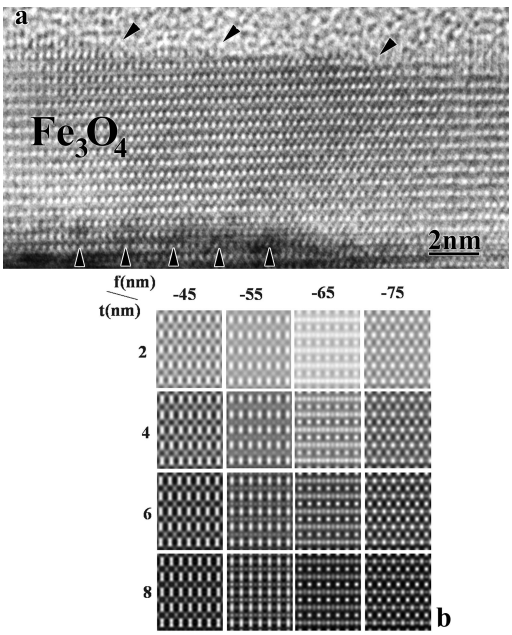

Fig. 6. HRTEM images of a Fe_3O_4 film along the $[11\bar{2}]$ direction. Dark contrast due to periodically strained regions at the interface near the lower edge as well as atomic steps at the oxide-glue interface near the upper edge are marked by arrows; (b) 300x300nm^2 STM image showing the characteristic morphology of a Fe_3O_4(111) film surface. U_t=1.4V, I_t=0.8nA. From Shaikhutdinov et al. [24]; (c) simulated thickness/defocus series for Fe_3O_4 projected along the $[11\bar{2}]$ direction (U=400kV, C_s=1.06mm, df=9nm, sc=0.72mrad).

the bright, slightly elongated spots in the micrograph correspond to the projection of the mixed trigonal layer consisting of Fe_{tet1}, Fe_{oct2} and Fe_{tet2} whereas the Kagome-layer Fe_{oct1} forms less intense round spots between the other two.

Six non-equivalent surface terminations are possible for the ideal Fe_3O_4 surface: two with tetrahedrally coordinated iron atoms, Fe_{tet1} and Fe_{tet2}, at the surface; two terminated by ocatahedrally coordinated iron atoms, Fe_{oct1} and Fe_{oct2}; and two terminated by the close-packed oxygen layers, O_1 and O_2 (compare Fig. 1). Experimentally, the surface with the Fe_{tet1} termination was found at the oxide-vacuum interface, relaxed in the [111] direction [24]. Although the high-resolution image in Fig. 6a shows clear lattice fringes even in the surface region, the presence of glue material makes a real surface structure analysis complicated. However, steps with height 0.48nm separated by flat terraces of different length are visible. They are marked with arrows in the upper part of Fig. 6a. For comparison, a typical STM image of a Fe_3O_4(111) film surface (from [25]) is presented in Fig. 6b. In agreement with the TEM results it shows atomically flat terraces with widths between about 5 and 100nm, separated by steps about 0.5nm high.

A high density of APBs may influence the magnetic properties of Fe_3O_4 [16]. APBs spaced several tens of nanometers apart were found in the films investigated here. One image of an APB is shown in Fig. 7a. A shift of (111) planes along the [111] direction was found to be 0.18nm. In order to determine the structure of the APB, image simulations were performed under the condition that the boundary is stoichiometric with respect to oxygen. The corresponding APB model is shown in Fig. 7b. In this model the Fe_{oct1} layer from the left domain is on the same level as the Fe_{tet1} layer from right the domain. The calculated image is shown as inset in Fig. 7a.

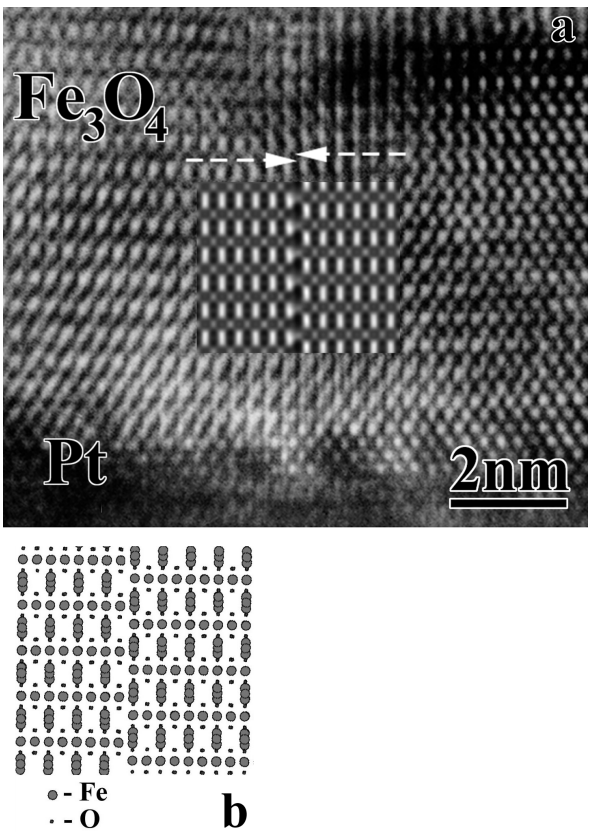

Fig. 7. HRTEM cross section image of an APB with a shift of 1.86Å along the [111] direction; the simulated image is shown in the inset; (b) projection of the corresponding atomic model of the APB along $[11\bar{2}]$.

APBs with a shift of 2.35Å were also observed in the film. It must be noted that the density of steps at the interface exceeds by far the density of APBs. As a rule, the oxide grows across Pt steps without formation of defects. The step height on Pt(111) is 2.26Å and the possible step heights of Fe_3O_4(111) at the interface are given by the separation of the iron layers which is either 1.82Å or 2.35Å. This step height mismatch may be accomodated by a deformation of the lattice planes. The presence of steps at the Pt surface may also lead to a local tilt of (111) planes and thus to the mosaic structure of the whole oxide film deduced from elongation (±1.5°) of the diffraction spots in Fig. 3b, c.

Summary

Epitaxial monocrystalline Fe_3O_4 thin films have been grown on Pt(111) substrates. No other iron oxide phases were detected by transmission electron microscopy. The film thickness variation from 5 to 7.5nm is attributed to nucleation and diffusion processes during oxidation. The films consist of [111] oriented single crystal domains randomly inclined with respect to the Pt [111] substrate by up to ±1.5°. This variation in the orientation is ascribed to the difference in the possible step heights of Pt(111) and Fe_3O_4(111) at the interface causing a measurable tilt in step-rich regions. From image simulations it is concluded that the first layer on top of the Pt substrate at the interface consists of iron. In order to improve the lattice match locally, the lattice parameters of Fe_3O_4 parallel to the interface varies by up to 2%. As a consequence, the strain varies periodically along the interface as visualized by contrast variations in the TEM images. The presence of steps at the Pt substrate occasionally gives rise to the appearance of APBs between single crystal domains with their (111) planes shifted by 1.82Å or 2.35Å with respect to each other along the [111] direction.

The present work shows that TEM is a useful technique in complement to LEED and STM for investigations of the growth mechanism and structure of the catalytic films. Specially, HRTEM technique combined with image simulation is the unique approach for the elucidation of the defect and interface structure of the model systems.

Acknowledgements

VVR is indebted to the Max-Planck-Society for his fellowship at the Fritz-Haber-Institut. The authors thank Dr. T. Gemming from the Max-Planck-Institut für Metallforschung, Stuttgart for the assistance with electron microscopy and Dr. A. Chuvilin from the Institute of Catalysis, Siberian Division, Russian Academy of Sciences for image simulation programs.

References

[1]. J.W. Geus, Appl. Catal. 25 (1986) 313.
[2]. M. Muhler, R. Schlögl, G.Ertl, J. Catal. 138 (1992) 413.
[3]. W. Weiss, D. Zscherpel, R. Schlögl, Cat. Let. 52 (1998) 215.
[4]. P.J. van der Zaag, R.M. Wolf, A.R. Ball, C. Bordel, L.F. Feiner, R.M. Jungblut, J. Magn. Magn. Mater. 148 (1995) 346.
[5]. J.C. Mallinson, The Foundation of Magnetic Recording, 2nd ed. (Academic, New York, 1993).
[6]. H.-J. Freund, Angew. Chem. 109 (1997) 444.
[7]. W. Weiss, G.A. Somorjai, J. Vac. Sci Technol. A 11 (1993) 2138.
[8]. K. Takeuchi, S.S. Perry, M. Salmeron, G.A. Somorjai, Surf. Sci. 323 (1995) 30.
[9]. A.B. Boffa, H.C. Galloway, P.W. Jacobs, J.J. Benitez, J.D. Batteas, M. Salmeron, A.T. Bell, G.A. Somorjai, Surf. Sci. 326 (1995) 80.
[10]. Sh.K. Shaikhutdinov, Y. Joseph, C. Kuhrs, W. Ranke, W. Weiss, Faraday Discuss. 114 (1999) 363.
[11]. J.M. Gaines, J.T. Kohlhepp, P.J.H. Bloemen, R.M. Wolf, A. Reinders, R.M. Jungblut, J. Magn. Mater., 165 (1997) 439.
[12]. T. Fujii, M. Takano, R. Katano, Y. Bando, Y. Isozumi, J. Appl. Phys. 68 (1990) 1735.
[13]. M. Ritter, H. Over, W. Weiss, Surf. Sci. 371 (1997) 245.
[14]. H.C. Galloway, J.J. Benitez, M. Salmeron, Surf. Sci. 298 (1993) 127.
[15]. C.S. Fadley, M.A. Van Hove, Z. Hussain, A.P. Kaduwela, J. Electron Spectrosc. Relat. Phenom. 75 (1995) 273.
[16]. M.L. Rudee, D.T. Margulies, E.A. Berkowitz, Microsc. Microanal. 3 (1997) 126.
[17]. G. Ketteler, W. Weiss, W. Ranke, R. Schlögl, Phys. Chem. Chem. Phys., (2001) 3 1114.
[18]. R.W.G. Wyckhoff, Crystal Structures, 2nd ed., Vol. I, Interscience, New York, 1982.
[19]. W. Weiss, M. Ritter, D. Zscherpel, M. Swoboda, R. Schlögl, J. Vac. Sci. Technol. A 16 (1998) 21.
[20]. W. Weiss, M. Ritter, Phys. Rev. B 59 (1999) 5201.
[21]. Th. Schedel-Niedrig, W. Weiss, R. Schlögl, Phys. Rev. B 52 (1995) 17449.
[22]. W. Ranke, M. Ritter, W. Weiss, Phys. Rev. B 60 (1999) 1527.
[23]. M Ritter, W. Ranke, W.Weiss, Phys. Rev. B 57 (1998) 7240.
[24]. M. Ritter, W. Weiss, Surf. Sci. 432 (1999) 81.
[25]. Sh. K. Shaikhutdinov, M. Ritter, X.-G. Wang, H. Over, W. Weiss, Phys. Rev. B 60 (1999) 11062.